Nitrosyliron(III) Hemoglobin: Autoreduction and Spectroscopy

Anthony W. Addison* and Joseph J. Stephanos
Chemistry Department, Drexel University, Philadelphia, Pennsylvania 19104
Received June 18, 1985; Revised Manuscript Received February 24, 1986

ABSTRACT: Nitrosyl complexes of the iron(III) forms of myoglobin, human hemoglobin, *Glycera dibranchiata* hemoglobins (Hb_m and Hb_h), and model iron(II) and iron(III) synthetic porphyrins including octaethylporphyrin (OEP) have been prepared. The iron(III) heme proteins are electron spin (paramagnetic) resonance (ESR) silent, while hexacoordinate solution structures are indicated for $[Fe(OEP)(NO)_2]ClO_4$ and for Hb_m(II)NO, which has an ESR spectrum similar to that of Mb(II)NO and the hexacoordinate iron(II) model complex Fe(OEP)NO(BzIm). The splitting of the α- and β-bands in the optical spectrum of Mb(III)NO and Hb_h(III)NO contrasts markedly with the sharp, single bands observed in that of Hb_m-(III)NO. The nondegeneracy of the d_{xz} and d_{yz} orbitals in Mb(III)NO and Hb_h(III)NO is attributed to the influence of the distal histidine. Circular dichroism spectra were obtained for Hb_m(III)NO, Hb_m(II)NO, Hb_h(III)NO, Hb_h(II)NO, Mb(II)NO, and Mb(III)NO. The vicinal chiral center contribution that governs the heme protein CD leads to low Kuhn anisotropies, which have been used to assign certain electronic transitions. The Hb(III)NO spectrum is not stable but transforms into that of Hb(II)NO. This autoredox process follows kinetics that are first order in $Fe^{III}NO$. The relative rates of autoreduction (25 °C, 1 atm NO) are Mb(III)NO < Hb_m(III)NO < Hb_α(III)NO < Hb_A(III)NO. At high NO partial pressure or after "recycling" of Hb_A, the rates of reduction decrease. The first step in the reaction of NO with the ferric heme is the reversible formation of the formally iron(III) adduct. This reacts with another molecule of NO, generating the final heme(II)–NO via nitrosylation of NO itself or of an endogenous nucleophile. Kinetic and spectroscopic evidence shows involvement of *trans*-heme–$(NO)_2$ in the reaction. The activation parameters $\Delta H^\ddagger$ and $\Delta S^\ddagger$ were determined. The overall reaction is photoenhanced.

Reactions of the heme proteins with nitric oxide continue to be extensively studied. Unlike the thermodynamically robust iron(II) heme nitrosyls, the iron(III) adducts show considerable variation in the lifetime of their stability. While the iron(III) forms of cytochrome P-450 and cytochrome *c* peroxidase are well established as being stable iron(III) nitrosyl adducts (O'Keeffe et al., 1978; Wayland & Olson, 1974; Yonetani et al., 1972; Ehrenberg et al., 1960), the history of the iron(III) nitrosyl [Fe(III)–NO] chemistry of hemoglobin and myoglobin is somewhat checkered (Sancier et al., 1962; Chien et al., 1969; Dickinson et al., 1971). For the reaction between Hb(III)[1] and NO, it was reported (Keilin & Hartree, 1937) that Hb(III)NO is formed reversibly, that its α/β-region spectrum is blue-shifted vs Hb(II)NO, and that it undergoes reduction of Hb(II)NO in the absence of oxygen. Ehrenberg and Szczepkowski (1960) showed that Mb(III) reacts with NO to yield Mb(III)NO, in which the α/β-bands are also blue-shifted with respect to Mb(II)NO. These workers stated that after 2 h, in the presence of NO, the adduct is transformed to Mb(II)NO. These observations are reiterated in a later paper (Chien, 1969), which however, implies that the reaction of NO with Hb(III) is essentially reductive rather than coordinative.

With the noteworthy heme pocket alterations in comparison with other Hb and Mb ($His^{E7} \rightarrow$ Leu, $Gly^{E6} \rightarrow$ Asp) (Imamura et al., 1972), *Glycera dibranchiata* monomeric Hb offers itself as an interesting model Hb for probing the chemical influences of the distal histidine. We report here the results of our studies on the reactions of NO with equine myoglobin, *G. dibranchiata* hemoglobin, and hemoglobin A and its subunits. During our pursuit of this work, other investigators have published results for related investigations of opossum hemoglobin and some other proteins (Sharma et al., 1983), including the autoredox reaction:

$$Fe^{III}NO \rightarrow Fe^{II}NO$$

Materials and Methods

Live *Glycera dibranchiata* were obtained from Woods Hole Marine Biological Laboratory. Erythrocytes were washed with 0.15 M Na_2SO_4–10 mM EDTA and lysed with distilled water. The heavy (oligomeric) and light (monomeric) Hb components (Hb_h and Hb_m) were separated by chromatography on Sephadex G-75. The buffer used throughout was pH 7 sodium phosphate/potassium phosphate (0.1 M, 1 mM EDTA, μ = 0.2).

Myoglobin was Sigma type III equine, human hemoglobin was Sigma type IV or from fresh human hemolysate, and other reagents were used as supplied by Sigma, Aldrich, and Fisher. Protein was assayed as the iron(II) carbonyl, with the published molar absorptivities (Seamonds et al., 1971; Addison & Burman, 1985). Hb_A was purified by passage through a Sephadex G-75 column (2 × 75 cm) at least twice to remove DPG (Imamura et al., 1969). Hemoglobin subunits were prepared according to Bucci and Fronticelli (1965) and Waks et al. (1973).

The protein nitrosyl complexes were obtained by flushing the methemoglobin solutions for at least 30 min with N_2

[1] Abbreviations: Hb_m, monomeric *G. dibranchiata* hemoglobin; Hb_h, oligomeric *G. dibranchiata* hemoglobin; Hb_A, human hemoglobin; Mb(II), iron(II) myoglobin; Mb(III), iron(III) myoglobin; DPG, 2,3-diphosphoglycerate; IHP, inositol hexaphosphate; SDS, sodium dodecyl sulfate; EDTA, ethylenediaminetetraacetate; DPPH, diphenylpicrylhydrazyl free radical; Acac, pentane-2,4-dione anion; Im, imidazole; MeIm, 1-methylimidazole; Dmim, 1,2-dimethylimidazole; BzIm, 1-benzylimidazole; TPP, tetraphenylporphyrin dianion; OEP, octaethylporphyrin dianion; PPIXDME, protoporphyrin IX dimethyl ester; ESR, electron spin (paramagnetic) resonance; CD, circular dichroism; MO, molecular orbital.

0006-2960/86/0425-4104$01.50/0

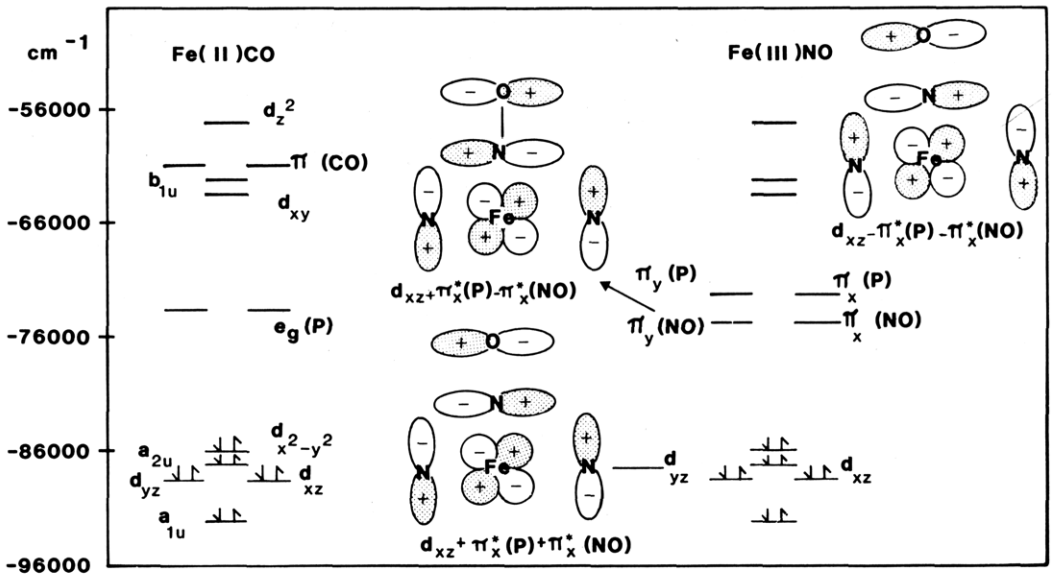

FIGURE 1: Molecular orbital scheme for Fe(III)NO, showing energies of the topmost filled and lowest empty orbitals. The linear combinations are $d_{xz,yz} = d_{xz,yz} + \pi^*_{x,y}(P) + \pi^*_x(NO)$, $\pi^*_{x,y}(NO) = d_{xz,yz} + \pi^*_{x,y}(P) - \pi^*_x(NO)$, and $\pi^*_{x,y}(P) = d_{xz,yz} - \pi^*_{x,y}(P) - \pi^*_x(NO)$.

(boil-off from MG Industrial Gases liquid N_2) followed by direct reaction of NO with the iron(III) protein. The NO (MG Industrial Gases) was scrubbed with 5 M KOH. The concentration of dissolved NO was calculated at the required temperature and pressure, with Henry's Law constants interpolated from the published values for aqueous buffer solutions (Armor, 1974; Shaw & Vosper, 1977). Experiments involving NO pressures greater than 1 atm were performed in a specially constructed Teflon-lined spectrophotometric cell (5.2-cm path length), which was pressure calibrated with a gas syringe.

After the autoreduction reaction was undergone, some samples of reduced Hb_A(II)NO were reoxidized with an excess of potassium hexacyanoferrate(III) to produce Hb_A(III)OH_2. The hexacyanoferrates were removed on a Sephadex G-75 column, and this "recycled" protein was also used, in separate kinetic experiments. Recycled Hb_A(III)OH_2 and several proteins of known molecular weight were compared at 4 °C by gel filtration on an analytical Sephadex G-75 column (1.5 × 93 cm), the eluent from which was monitored spectrophotometrically at 280 nm.

Fe(OEP)NO^+Cl^- was prepared by dissolving Fe(III)-(OEP)Cl in degassed toluene in vacuo, followed by admission of nitric oxide. In the presence of MeOH or stoichiometric Im, MeIm, Dmim, or BzIm, the final product was Fe^{II}-(OEP)NO. Overnight stirring of Fe^{III}(OEP)Cl in toluene over aqueous dithionite (pH 7) followed by passage of nitric oxide yielded Fe^{II}(OEP)NO. Fe(OEP)NO(BzIm) was formed in a like fashion, from the reaction of Fe(OEP)NO^+ with excess BzIm. The dinitrosyl Fe(OEP)$(NO)_2ClO_4$ was prepared in solution by stirring a mixture of Fe(OEP)Cl and $AgClO_4$ in toluene overnight under NO, while Fe(PPIXDME)$(NO)_2ClO_4$ was prepared similarly by treating Fe(PPIXDME)$(OOCCH_3)$ (Ainscough et al., 1978) with $HClO_4$ and NO.

Visible spectra and kinetic data were recorded on Perkin-Elmer 320 and Lambda-3 spectrophotometers thermostated to ±1 °C. Electron spin resonance spectra were obtained at 77 K on a Varian E-12, X-band spectrometer, calibrated near $g = 2$ with DPPH and $VO(Acac)_2$. The CD spectra, reported in terms of $\Delta\epsilon$ vs. λ, were obtained on a Jasco J41C instrument. The absorption and CD data were digitized mechanically, and the Kuhn anisotropy spectra (Gillard, 1968; Addison & Dougherty, 1981) were computer-generated and plotted as $\Delta\epsilon/\epsilon$ vs. λ. Error limits on derived quantities are quoted as $\pm\sigma$.

Results and Discussion

All the proteins investigated herein form iron(III) nitrosyls that are of sufficient stability at ambient temperature that they can be characterized spectroscopically. Our interpretations of these observations are now outlined, using an electronic structure model as a basis.

Electronic Structure. The electronic charge redistribution on binding of NO to an iron(III) heme is toward iron(II) (d^6-NO^+) in both the proteins and the models (Wayland & Olson, 1974). The Fe(III)–NO systems are isoelectronic with the corresponding Fe(II)–CO ones, having a total of six electrons associated with the metal d and ligand π^* orbitals, so that a linear Fe(III)–NO linkage is observed in the absence of any distal perturbations (Scheidt et al., 1984; O'Keeffe et al., 1978; Hoffman & Gibson, 1978). This has been attributed to the π-bonding involving the unpaired electron in the π^*(NO) orbital, as may the greater strength of the Fe(III)–NO vs. Fe(II)–CO bond (Benko & Yu, 1983). In contrast, the more commonly studied $Fe^{II}NO$ unit has a bent structure (Deatherage & Moffat, 1979; Scheidt & Piciulo, 1976).

In any scheme for the electronic structure of these types of systems, the possibility of d_π-electron back-donation from the occupied metal d_{xz} or d_{yz} orbital to the empty $e_g(\pi^*_{x,y})$ orbitals of the porphyrin must be taken into account (Smith & Williams, 1970). This would raise the e_g orbitals and lower the d_π orbital, so that the last now becomes bonding, as verified by the shift to higher energy of the α-bands [$a_{2u} \rightarrow e_g$ (π^*-P)] (P denotes porphyrin) observed in $Fe^{II}CO$ (17 600 cm^{-1}) and $Fe^{III}NO$ (17 400 cm^{-1}), in comparison to the value calculated from extended Hückel orbital energies [$a_{2u} \rightarrow e_g$(P)] [13 120 cm^{-1} without d_{xz}–e_g(P) mixing; Smith & Williams, 1970; Eaton et al., 1978].

In order to model the nitrosyliron(III) hemoglobin chromophore, we have therefore (for the sake of simplicity) empirically modified the extended Hückel orbital energy scheme (Figure 1) for (carbonmonoxy)hemoglobin (Eaton et al., 1978),[2] approximating the Fe environment by C_{4v} symmetry. The major perturbation to the scheme in passing from CO to

[2] The less common convention is used, in which the d_{xy} orbital is directed toward the N donor atoms.

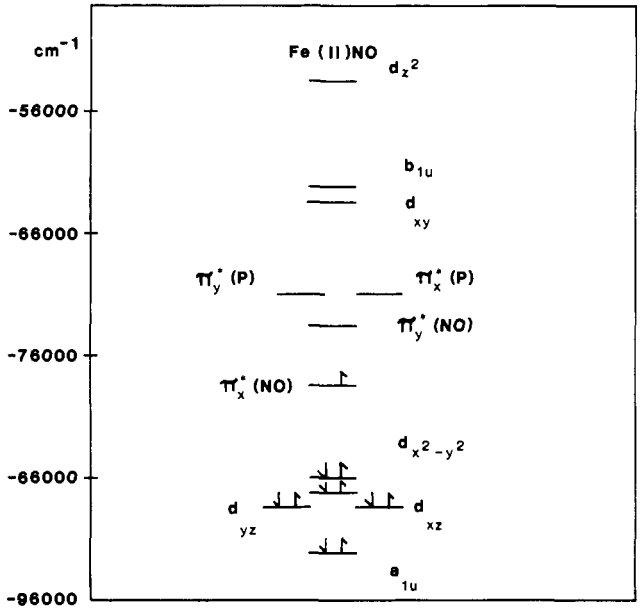

FIGURE 2: Energies of the upper filled and lower empty molecular orbitals for Fe(II)NO. The linear combinations are $d_{xz,yz} = d_{xz,yz} + \pi^*_{xy}(P)$, $\pi^*_x(NO) = d_{z^2} + \pi^*_x(NO)$, $\pi^*_{xy}(P) = d_{xz,yz} - \pi^*_{xy}(P)$, and $d_{z^2} = d_{z^2} - \pi^*_x(NO)$.

NO is that the doubly degenerate π^* MO of the free NO molecule is at considerably lower energy (−74 730 cm^{-1}; Linn et al., 1980) and thus close to the porphyrin $e_g(\pi^*)$ orbital at −74 440 cm^{-1} (Eaton et al., 1978).

Further modification of the Hb(III)NO MO scheme gives that for $Fe^{II}NO$ (Figure 2), which uses the selection rules for C_s symmetry. The bent $Fe^{II}NO$ structure in the xz plane suggests that depiction of overlap between the iron d_{z^2} orbital and the singly occupied $\pi^*_x(NO)$ orbital is appropriate.

Principal features of these schemes are that the linear $Fe^{II}NO$ unit maximizes $d_\pi(Fe)$–$\pi^*(NO)$ bonding, while bending of the $Fe^{II}NO$ unit removes the $\pi^*(NO)$ double degeneracy to produce one MO with essentially $\pi^*_y(NO)$ character and a second $\pi^*_x(NO)$ orbital appropriate for σ-bonding with the metal d_{z^2} orbital. Indeed, a Jahn–Teller bending distortion of the $Fe^{II}NO$ fragment is expected when either or both the metal d_{z^2} and the $\pi^*(NO)$ levels are partially occupied. It seems that the Fe–NO bond strength will depend on the relative importance of the σ-electronic system (which is maximized at about 120°) and π-back-bonding, which maximizes at 180° (Cotton & Wilkinson, 1980). ESR results for heme–$Fe^{II}NO$ systems place 53% of the unpaired spin population in the $\pi^*(NO)$ level (Doetschman et al., 1980), clearly demonstrating the mixing between $\pi^*_x(NO)$ and $d_{xz}(Fe)$.

ESR Spectra. The ESR spectra of $Hb_m(II)NO$ (Figure 3) and $Hb_m(III)NO$ show that the former is paramagnetic, having an ESR spectrum similar to that of other Hb and Mb(II)NO systems and falling into the "type 2" classification of Yonetani et al. (1972), with $g = 1.97$, 2.03, and 2.06. This indicates that it is a low-spin nitrosyl, similar to the six-coordinate iron(II) model complexes Fe(OEP)NO(BzIm) (Figure 3) and Fe(TPP)NO (piperidine) (Wayland et al., 1974).

The ESR is responsive to the state of the coordination site trans to NO, so that the normally coordinated proximal histidine imidazole thus transmits information about the conformational state of the protein (Yoshimura et al., 1971). If the conformational equilibrium of $Hb_A(II)NO$ is shifted from the R to the T state by addition of DPG, IHP, SDS, or ATP

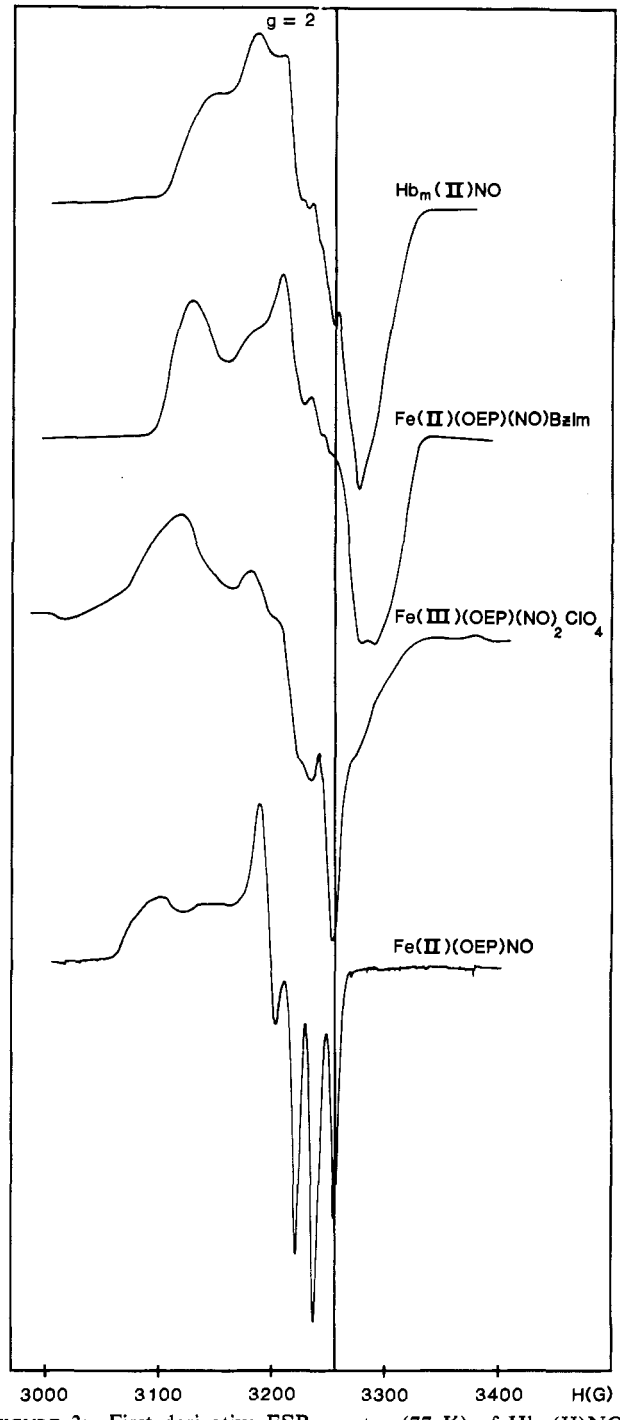

FIGURE 3: First derivative ESR spectra (77 K) of $Hb_m(II)NO$, Fe(OEP)NO(BzIm), $Fe(OEP)(NO)_2ClO_4$ and Fe(OEP)NO.

or by changes in pH, the resulting tensions break the Fe–N(proximal His) bond (Trittelvitz et al., 1975; Szabo & Perutz, 1976; Ascenzi et al., 1981; Mackin et al., 1983). However, on the addition of DPG, IHP, SDS, or $Fe(CN)_6^{3-}$ at pH 7 or the lowering of the pH to 5.5, the spectrum of $Hb_m(II)NO$ does not change; thus, no changes of the coordination state occur under such conditions. This appears to contrast with recent findings for the dependence of the carbonyl–heme structure on the pH (Satterlee, 1984).

The pronounced ^{14}N-hyperfine features around $g = 2.00$ in the spectrum of Fe(OEP)NO indicate the pentacoordinate structure, while a hexacoordinate structure is indicated for $Fe(OEP)(NO)_2ClO_4$ (Figure 3). The fact that the nitrosyls of ferric hemes are ESR-silent is consistent with the scheme in Figure 1.

Table I: Absorption Spectral Data for Nitrosyl Complexes of Hb_A, Hb_α, Hb_β, Mb, Hb_m, and Hb_h

	λ (nm) [$10^{-3}\epsilon$ (M^{-1} cm^{-1})]					
	α		β		γ	
heme	Fe(II)	Fe(III)	Fe(II)	Fe(III)	Fe(II)	Fe(III)
$Hb_\alpha NO$	566	562	536	532	418	411
$Hb_\beta NO$	572	568	542	538	417	416
$Hb_A NO$	572 [13]	566 [11]	544 [12.6]	533 [11.7]	418 [130]	415 [126]
MbNO	579 [9.9]	574 [12.5]	546 [10.9]	532 [12.7]	422 [148]	421 [150]
$Hb_m NO$	578 [15.7]	572 [20.3]	545 [15.1]	524 [16.3]	420 [140]	418 [81.9]
$Hb_h NO$	572 [13.9]	566 [18.9]	542 [15.0]	524 [17.7]	416 [111]	417 [150]
$Hb_m(NO)_2$[a]		562		527		436
$Fe(PPIXDME)(NO)_2^+$[b]		560		525		
$Fe(OEP)(NO)_2^+$[c]		557		529		

[a] Hb_m(III) under 4 atm of NO vs. Hb_m under 1 atm of NO. [b] In toluene. [c] In tetrahydrofuran.

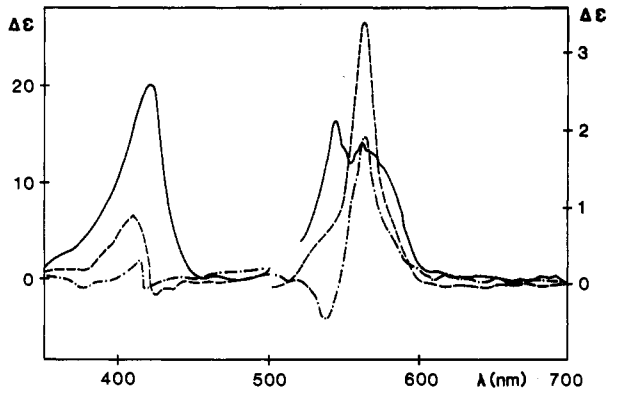

FIGURE 4: Circular dichroism of Hb_m(III)NO (-·-), Hb_h(III)NO (--), and Mb(III)NO (-).

Electronic Spectra. In Table I are summarized the spectral data in the visible (450–650-nm) and Soret (390–450-nm) regions for the nitrosyl complexes of Mb, Hb_m, Hb_h, Hb_A, and the subunits Hb_α and Hb_β. The optical spectra of these nitrosyls, as is usual for heme protein adducts, are quite characteristic, as the α/β-region absorption is relatively sharp and split into two envelopes, each within 2 nm of 544 and 575 nm with $10 < 10^{-3}\epsilon < 15$ M^{-1} cm^{-1}. These (Q-) bands arise from the doubly degenerate $a_{2u} \rightarrow e_g$ transitions of the porphyrin, polarized in the *xy* plane of the heme (Platt, 1956).

CD spectra for MbNO, Hb_mNO, and Hb_hNO are also given in Figures 4 and 5. In the α/β-region, both Hb_m(III)NO and Hb_m(II)NO exhibit a positive Cotton effect at 563 and 590 nm and a negative one at 537 and 549 nm respectively. Unlike Hb_h(III)NO and Hb_h(II)NO, where only one distinct dichroic band is evident at 568 and 571 nm (shoulder at 531 and 529 nm), Mb(III)NO and Mb(II)NO each show two distinctly positive dichroic bands at 563 and 586 nm and 547 and 545 nm. The Soret dichroic bands of Hb_m(III)NO, Hb_m(II)NO, Hb_h(III)NO, and Hb_h(II)NO show a negative Cotton effect of low magnitude, while in contrast Mb(III)NO and Mb(II)NO show strongly positive Cotton effects. Dipolar interactions between the heme $\pi \rightarrow \pi^*$ transitions and those of nearby aromatic groups are responsible for a large part of the induced rotational strengths of the heme transitions in this region (Hsu & Woody, 1971). Presumably, the distribution of the aromatic amino acid residues with respect to the heme group produces wavelength shifts, which thus influence the positive CD component to dominate the negative one.

The optical spectra of nitrosylhemes, like those of most closed-shell metal porphyrins, generally only exhibit ($\pi \rightarrow \pi^*$) Q-, B-, and N-bands. In contrast, the CD spectra seem to be richly structured in this regard (Figures 4 and 5). A number of bands and shoulders are observed in the CD spectra of the nitrosyls, which are not necessarily associated with the porphyrin Q- and B-bands that dominate the simple absorption in this region. These appear more likely to be charge transfer rather than d–d in character. In Figure 6, we used the criteria of weak absorption and large Kuhn anisotropy factor to characterize the nature (electric dipole forbidden, magnetic dipole allowed) of these transitions (Tables II and III). The vicinal chiral center contribution (Hawn et al., 1979) that governs the heme protein CD apparently leads generally to low Kuhn anisotropies ($g = 10^{-3}$ for magnetic dipole allowed, 10^{-4} for forbidden). The proposed assignments fit the observed spectra quite well, when the selection rules for CD are taken into account and corrections for exchange interactions are made; an exchange energy (Zerner et al., 1966) of 4030 cm^{-1} was added to the orbital energy difference for the Fe(d) $\rightarrow$ π^*(P), π(P) $\rightarrow$ NO(π^*), and Fe(d) $\rightarrow$ NO(π^*) transitions. For the d $\rightarrow$ d transitions, the exchange energy given by a

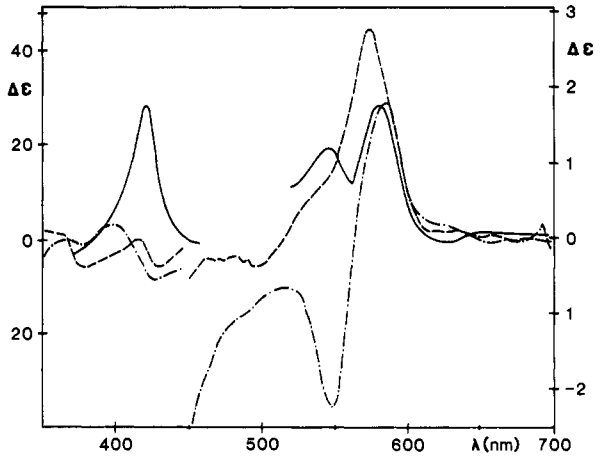

FIGURE 5: Circular dichroism of Hb_m(II)NO (-·-), Hb_h(II)NO (--), and Mb(II)NO (—).

Table II: Orbital Origins of Transitions in Iron(III) Heme Nitrosyls

orbital promotion	calcd energy, $10^{-3}\nu$ (cm^{-1})	obsd energy, $10^{-3}\nu$ (cm^{-1}) ($10^4 g$)		
		Mb(III)-NO	Hb_m(III)-NO	Hb_h(III)-NO
$d_{x^2-y^2} \rightarrow \pi^*_y$(P)	15.6	15.6		
$a_{2u} \rightarrow \pi^*_y$(NO)	16.8		16.5 (0.28)	16.8 (0.4)
$d_{xz} \rightarrow \pi^*_x$(P)	17.1	17.1 (1.2)	17.3 (0.72)	17.1 (0.7)
$a_{2u} \rightarrow \pi^*_x$(P)	17.2	17.3	17.5	17.2
$a_{1u} \rightarrow \pi^*_x$(NO)	18.6	17.8 (1.3)	17.8 (1.2)	17.9 (5.3)
$a_{2u} \rightarrow \pi^*_y$(P)	18.9	17.9		17.7
$d_{yz} \rightarrow \pi^*_y$(NO)	20.8	18.3	21.3 (0.6)	20.2 (0.7)
$d_{yz} \rightarrow \pi^*_y$(P)	21.1	20.0 (0.61)		
$a_{1u} \rightarrow \pi^*_y$(NO)	22.6	21.7 (0.6)	22.3	22.5 (-0.1)
$d_{x^2-y^2} \rightarrow b_{1u}$	22.8	22.9 (2.1)		
$a_{1u} \rightarrow \pi^*_x$(P)	22.9	23.8	23.8	24.0
$a_{2u} \rightarrow d_{xy}$	23.9	24.3 (1.9)	24.0 (0.1)	24.0 (0.33)
$d_{x^2-y^2} \rightarrow d_{xy}$	25.2		24.9 (6.3)	24.8

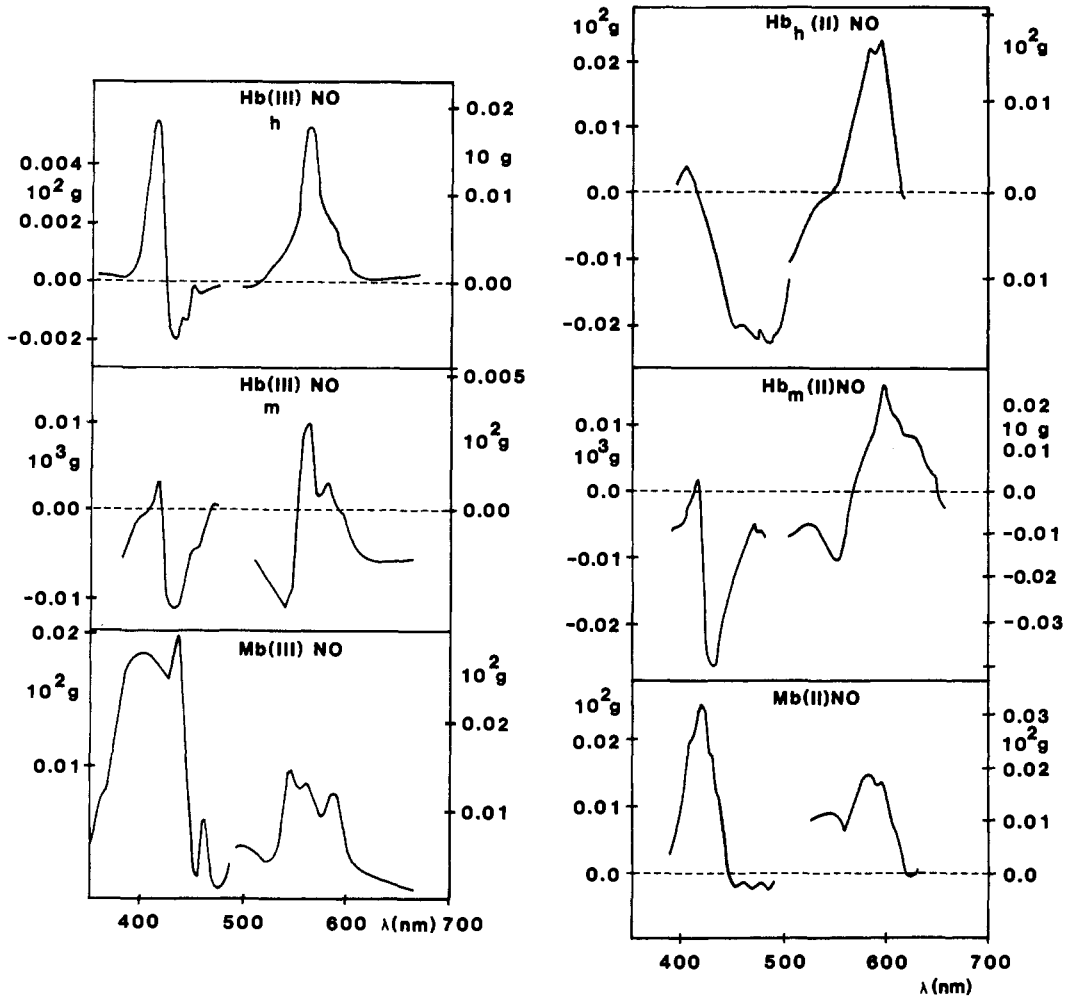

FIGURE 6: Kuhn anisotropy spectra for Hb_m(III)NO, Hb_m(II)NO, Hb_h(III)NO, Hb_h(II)NO, Mb(III)NO, and Mb(II)NO.

Table III: Orbital Origins of Transitions in Iron(II) Heme Nitrosyls

orbital promotion	calcd energy, $10^{-3}\nu$ (cm^{-1})	obsd energy, $10^{-3}\nu$ (cm^{-1}) ($10^4 g$)		
		Mb(II)NO	Hb_m(II)-NO	Hb_h(II)NO
$a_{1u} \rightarrow \pi^*_x(NO)$	14.6	14.6 (3)	14.4 (2)	14.6 (0.19)
$d_{x^2-y^2} \rightarrow \pi^*_y(P)$	15.3		14.8 (−0.1)	
$d_{x^2-y^2} \rightarrow \pi^*_x(P)$	15.6	14.8 (3)	15.6 (0.49)	15.8 (0.6)
$\pi^*_x(NO) \rightarrow b_{1u}$	15.6	16.2 (0.4)	16.1 (1.3)	
$a_{2u} \rightarrow \pi^*_y(P)$	16.9	16.9 (1.7)	16.6 (1.9)	16.7 (1.3)
$d_{yz} \rightarrow \pi^*_y(NO)$	17.1	17.1 (1.9)	16.9 (2.5)	17.0 (2.2)
$a_{2u} \rightarrow \pi^*_x(P)$	17.2	17.3	17.5 (0.74)	17.3 (2.2)
$a_{1u} \rightarrow \pi^*_y(NO)$	18.9	18.4 (1.2)	19.0 (−0.7)	17.9 (1.3)
$d_{yz} \rightarrow \pi^*_y(P)$	20.8	20.5 (1.2)		19.1 (3.1)
$d_{xz} \rightarrow \pi^*_x(P)$	21.1	20.9 (−0.2)	21.1	20.7 (−2)
$a_{1u} \rightarrow \pi^*_y(P)$	22.6	21.7 (−2)	23.3 (1.8)	21.7 (−2)
$a_{1u} \rightarrow \pi^*_x(P)$	22.9	23.7	23.8	24.0
$a_{2u} \rightarrow d_{xy}$	23.9	23.8 (2.5)		
$d_{x^2-y^2} \rightarrow d_{xy}$	24.4		24.6 (−0.2)	25.5 (−0.1)

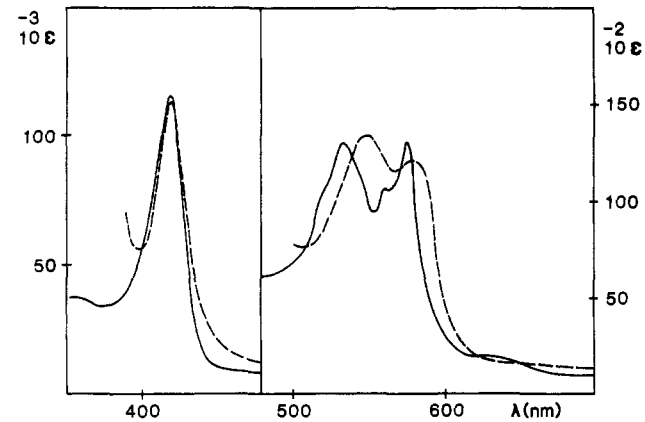

FIGURE 7: Optical absorption spectra of Mb(III)NO (—) and Mb(II)NO (--) at pH 7, 25 °C.

crystal field computation was used (Eaton et al., 1978; Otsuka, 1966), though the transition energy is essentially just the difference between the energies of the donor and the acceptor orbitals.

The splitting of the α/β-bands (Q-bands) in the optical spectra of Mb(III)NO and Hb_h(III)NO (Figures 7 and 8) at 561 and 581 nm (shoulder) contrasts markedly with the sharp, single band observed in Hb_m(III)NO. We attribute this splitting to nondegeneracy of the $e_g(\pi^*_{x,y})$ orbitals of the porphyrin in Mb(III)NO and Hb_h(III)NO resulting from the d_{xz}, d_{yz} nondegeneracy under the influence of the distal histidine. The CD spectra of Hb_m(III)NO and Hb_m(II)NO have only one absorption band in the α-region, indicating that the x and y components of the Q transitions are probably close to degenerate. O'Connor et al. (1980) have proposed that the positive and the negative ellipticities observed for Hb_m may result from the x and y components of the $a_{2u} \rightarrow e_g$ absorption gaining rotational strengths of opposite sign (despite the 30-nm separation observed between the two features). It seems that the x and y components in the case of MbNO and Hb_hNO are nondegenerate as a consequence of the d_{xz}, d_{yz} nondegeneracy as discussed above and have only a positive rotational strength. The differences in the rotational strength between Hb_m and both Mb and Hb_h are clearly characteristic of their active site differences.

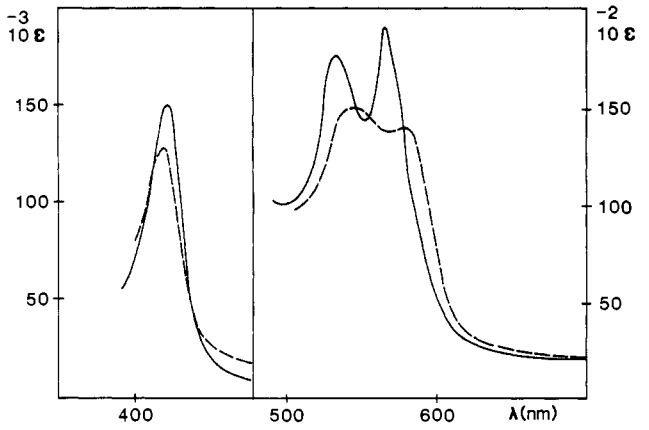

FIGURE 8: Optical absorption spectra of $Hb_h(III)NO$ (—) and $Hb_h(II)NO$ (--) at pH 7, 25 °C.

Table IV: Comparison of Electronic Promotions of Hb_AO_2, Hb_ACO, Hb(II)NO, and Hb(III)NO

orbital promotion	Hb_AO_2[a]	Hb(II)-NO	Hb(III)-NO	Hb_ACO[a]
$d_{x^2-y^2} \rightarrow e_g(\pi^*$ ligand)	10000	15280	15570	29000
$a_{2u} \rightarrow e_g(\pi^*$ ligand)	4000	16800	16900	26000
$d_\pi \rightarrow e_g(\pi^*$ ligand)	10000	17000	17200	30000
$a_{2u} \rightarrow e_g(\pi^*$ prophyrin)(α)	17300	17500	17400	17600
$d_\pi \rightarrow e_g(\pi^*$ porphyrin)	19000	21000	20800	14000
$a_{1u} \rightarrow e_g(\pi^*$ ligand)	7000	23000	22600	32000
$a_{1u} \rightarrow e_g(\pi^*$ porphyrin)(γ)	24100	23800	23800	23900
$a_{2u} \rightarrow d_{xy}$	22500	23900	23900	24900
$d_{x^2-y^2} \rightarrow d_{xy}$	22000	24000	25000	25100

[a] Eaton et al., 1978.

The weak intensity of the $d_\pi \rightarrow e_g(\pi^*$-porphyrin) transition is consistent with the essentially electric dipole forbidden character of this electronic promotion. The electronic and the CD spectra indicate therefore that the fourfold degeneracy of the $d_\pi \rightarrow e_g(\pi^*)$ transitions in the case of both oxidation states of the MbNO and the Hb_hNO is lifted by deviation of the NO ligand from the perpendicular to the porphyrin plane.

Nitrosyl metalloporphyrins have charge-transfer absorptions (Antipas et al., 1978) of the type $a_{1u} \rightarrow \pi^*_{x,y}(NO)$–$d_{xz,yz}$ near 24300 cm^{-1}, and the absorption data (Table IV) for our systems [$a_{1u} \rightarrow \pi^*_{x,y}(NO)$–$d_{xz,yz}$] at 23000 cm^{-1} are in agreement with this result. For $Hb_A(II)O_2$, the charge-transfer band $d_\pi \rightarrow e_g(\pi^*$-$O_2)$ (10000 cm^{-1}) has moved to shorter wavelengths in Fe(II)NO [$d_\pi \rightarrow e_g(\pi^*)$ (17000 cm^{-1})], in Fe(III)NO [$d_\pi \rightarrow e_g(\pi^*)$ (17200 cm^{-1})], and in Fe(II)CO [$d_\pi \rightarrow e_g$ (π^*-CO) (30000 cm^{-1})] (Eaton et al., 1978), as the result of the decreasing π-acceptor ability: $O_2 > NO > CO$. Figures 4 and 5 indicate that the $d_{x^2-y^2} \rightarrow d_{xy}$ and $d_\pi \rightarrow d_{z^2}$, d_{xy} ligand-field transitions are expected at considerably higher energy.

Kinetic Studies. The $Hb_m(III)NO$ spectrum is not stable (Figure 9) but transforms into that of $Hb_m(II)NO$. Under 1 atm NO pressure, this autoredox process follows kinetics pseudo first order in [$Hb_m(III)NO$], with a pseudo-first-order rate constant k_1' of 2.17×10^{-4} s^{-1} (pH 7, 25 °C; Table V). Figure 9 evidences that the known charge (isoelectric) dispersity in Hb_mNO (Addison et al., 1980; Kandler et al., 1984) is not connected to any significant kinetic dispersity, as the system exhibits simple pseudo-first-order behaviour for over four half-lives. In the case of Mb(III)NO, the autoredox reaction rate (Table V) may be slightly less than previously reported (half-life ca. 1500 s; Ehrenberg & Szczepkowski, 1960), following a rate law again first order in Mb(III)NO,

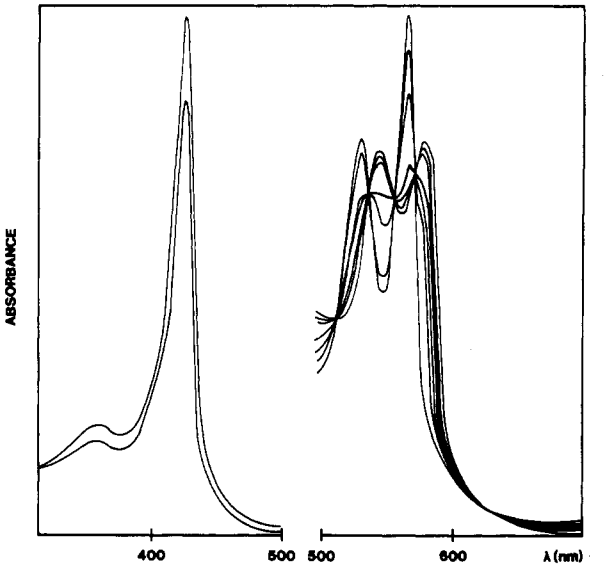

FIGURE 9: Spectral time course (15-min intervals) for the reaction of $Hb_m(III)NO$ with NO in deoxygenated 0.1 M phosphate buffer, pH 7.0, 25 °C, 1.0 atm of NO.

Table V: Pseudo-First-Order Rate Constants and Derived Kinetic Parameters for Reaction of NO with $Hb_m(III)NO$ and Mb(III)NO

$Hb_m(III)NO$[a]		Mb(III)NO	
[NO] (mM)	$10^4 k_1'$ (s^{-1})	[NO] (mM)	$10^4 k_1'$ (s^{-1})
0.87	1.32 ± 0.01	0.87	0.54 ± 0.01
1.14	1.59 ± 0.02	1.02	0.64 ± 0.02
1.54	2.07 ± 0.04	1.14	0.75 ± 0.03
1.72	2.17 ± 0.04	1.73	1.04 ± 0.03
1.74	2.33 ± 0.05	2.03	1.21 ± 0.03
2.53[b]	2.75 ± 0.06	2.46	1.42 ± 0.04
3.65	3.44 ± 0.05	2.69	1.55 ± 0.05
5.45	3.95 ± 0.05		
8.77	5.24 ± 0.06		
10.6	5.55 ± 0.08		
12.8	5.86 ± 0.08		

const	$Hb_m(III)NO$	Mb(III)NO
k_4 (s^{-1})[c]	$(7.5 \pm 0.5) \times 10^{-4}$	$(1.1 \pm 0.6) \times 10^{-3}$
K_2[c]	$(2.46 \pm 0.07) \times 10^2$	59 ± 2
k_3 (s^{-1})[d]	0.154 ± 0.004	0.056 ± 0.003
K_2[d]	2.1 ± 0.1	<1[e]

[a] One data point was rejected at the >99% confidence level. [b] Correction to p_{NO} made for dissolved NO at all $p_{NO} > 1$ atm. There is little evidence to be found for NO dimerization under similar conditions [Melia (1965) and references cited therein], and fugacity corrections are of little significance, particularly above the critical temperature (Hildebrand et al., 1970). [c] First mechanism. [d] Second mechanism. [e] $\sigma(K_2) > K_2$.

with $k_1' = 1.04 \times 10^{-4}$ s^{-1} (pH, 7, 25 °C, 1.0 atm NO). We perceive two probable reasons (apart from temperature differences) for any discrepancy in rates between our experiments and those of previous workers. First, our buffer system contains EDTA so that adventitious free Cu^{2+} [which catalyzes autoredox conversion of heme proteins (Rifkind et al., 1976)] is essentially absent. Second, our k_1' for the hemes was measured at low light levels (spectrophotometer). Indeed, when Mb(III)NO is subjected to medium-intensity broad-band illumination (quartz–iodine projector lamp, 17 °C), the overall observed rate of redox conversion is more than twice the purely thermal value at 23 °C. The same type of photoenhancement occurs for $Hb_m(III)NO$, while no photoreduction is observed in the absence of NO.

By way of contrast with the results for the monomeric proteins, experiments with Hb_A reveal that the situation is not exactly as one would infer from the literature. Under con-

Scheme I

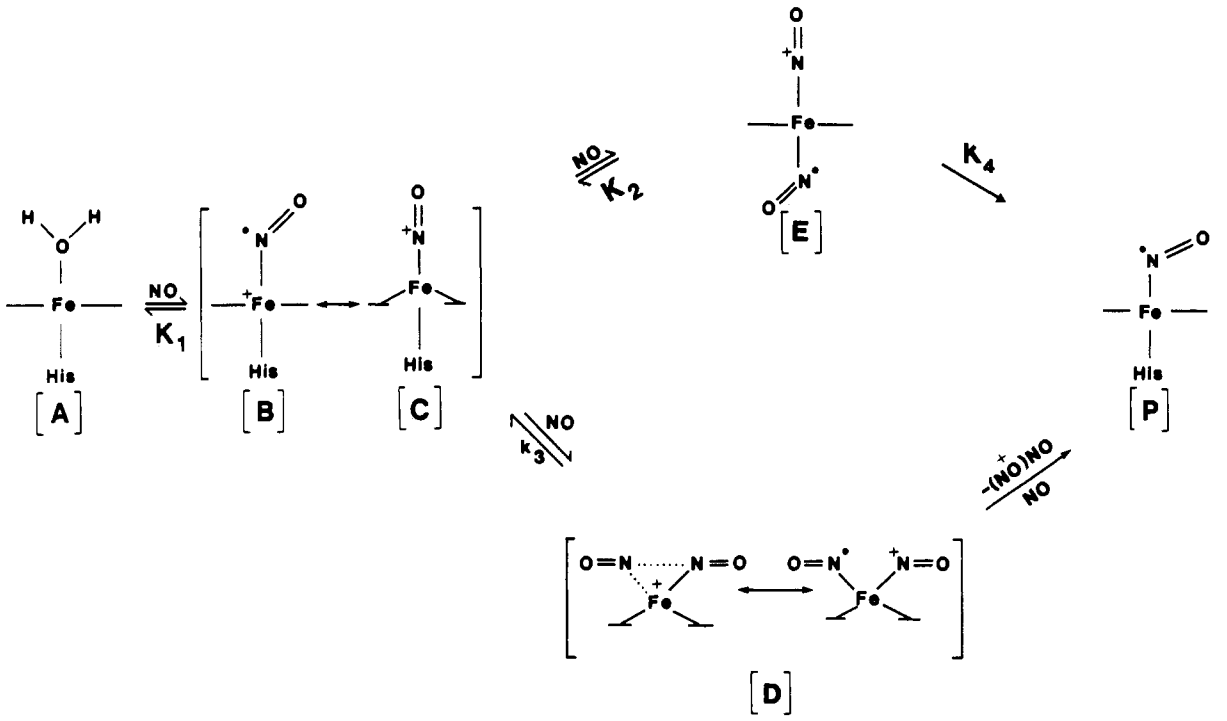

ditions as described above, Hb_A(III)NO is converted to Hb_A(II)NO with $k_1' = 9.67 \times 10^{-4}$ s^{-1}. Contrary to a previous implication (Chien, 1969), nitrosylation of Hb_A(III)(OH_2) thus indeed yields the iron(III) nitrosyl (Keilin & Hartree 1937; Sancier et al., 1962), although unique isosbestic points are not observed during the subsequent autoredox conversion of the native tetrameric protein.

After "recycling" of Hb_A(II)NO, the pseudo-first-order rate constant decreases markedly, to $k_1' = 0.18 \times 10^{-4}$ s^{-1}, isosbestic points occurring at 563 and 534 nm. The autoreduction of Hb_α(III)NO also follows pseudo-first-order kinetics, with $k_1' = 9.0 \times 10^{-4}$ s^{-1} (pH 7, 25 °C, 1.0 atm NO), showing isosbestic points at 580 and 520 nm. Denaturation prevented our obtaining satisfactory kinetic data for the β-chains.

Although NO is kinetically the reductant in the monomeric systems, it appears that consequent chemical modification of the protein may be involved in Hb_A, as recycling the protein through the redox step results in a rate decrease after the initial cycle. Both Lys and His (present in the distal environment) can presumably be nitrosylated (Müller et al., 1960; Fish et al., 1976). The K_{av} value (Sephadex G-75) of Hb_A is not affected by the recycling process.

The first step in the reaction of NO with the heme iron(III) (A) (Scheme I) is reversible formation (K_1) of the heme$^+$–NO (B), for which the optical and ESR studies (Wayland & Olson, 1974; Yonetani et al., 1972; Mertis & Wilkinson, 1976) suggest that the spin-paired nitrosonium–iron(II) formulation (C) is more appropriate. This nitrosonium–heme (C) is well modeled by species such as Fe(OEP)NO$^+$Cl$^-$, which is formed in the first step of the reaction of Fe(OEP)Cl with NO. In this higher oxidation state, Fe(OEP)NO$^+$Cl$^-$ is preferentially stabilized by the π-donor character of the chloride ligand (Porterfield, 1984), while the lower oxidation state heme(II)–NO will be preferentially stabilized by the π-acceptor character of the imidazole.

Our kinetic studies show that the protein nitrosonium–heme (C) reacts with one additional molecule of NO in the rate-determining step. The dependence on [NO] is not a consequence of the equilibrium K_1, as we have found the protein $Fe^{III}NO$ species to be fully formed at $p_{NO} < 0.02$ atm, a pressure greatly exceeded in all the kinetics.

An important feature of the observed kinetics is that at higher NO partial pressures (up to ca. 7.5 atm) the observed reaction rates of Hb_m(III)NO and Mb(III)NO are actually markedly less than the values that would be expected on the basis of a simple first-order [NO] dependence deduced from the lower pressure data. Complexity in the kinetics has been noted previously (Sharma et al., 1983). However, the raw kinetic data alone do not distinguish between two possible reaction pathways (Scheme I).

In the first mechanism, the additional NO displaces the proximal histidine imidazole in an equilibrium process (K_2) and forms the *trans*-dinitrosylheme (E). If this undergoes overall loss of NO$^+$ by reaction (k_4) with H_2O or another endogenous nucleophile (vide ultra Hb_A), then the resulting nitrosyliron(II) heme will rapidly re-form the proximal linkage (in P). The conventional rate law for a process with preequilibrium then applies:

$$d[P]/dt = k_4[Hb(III)][NO]/(K_2^{-1} + [NO])$$

At lower [NO], the formation of E would be rate-limiting and the reaction would be first order in [NO], with the observed pseudo-first-order rate constant $k_1' = k_4K_2[NO]$. At higher [NO], k_4 is the rate-limiting step, and the rate approaches $k_1' = k_4$. Inadequate stability of the 1:1 Fe(III)–imidazole adducts interferes with the observability of the K_2 step in a simple model system in the presence of imidazoles.

In the second mechanism, the rate-determining step is NO attack at the already coordinated NO, so that a heme of the type D is formed, for which process the overall second-order rate constant is k_3. If such a transition-state complex approaches twofold symmetry, then the other resonance forms actually depicted must be considered. Notable examples of tetrapyrrolic complexes with this geometry include Mo(TPP)O_2 (London & Bennet, 1979; Mentzen et al., 1980), Ti(TPP)O_2 (Guilard et al., 1976), Ti(phthalocyanine)Cl_2 (Goedken et al., 1985), Mn(TPP)O_2 (Hoffman et al., 1976), and Fe(TPP)O_2 (Welborn et al., 1981; McCandlish et al., 1980).

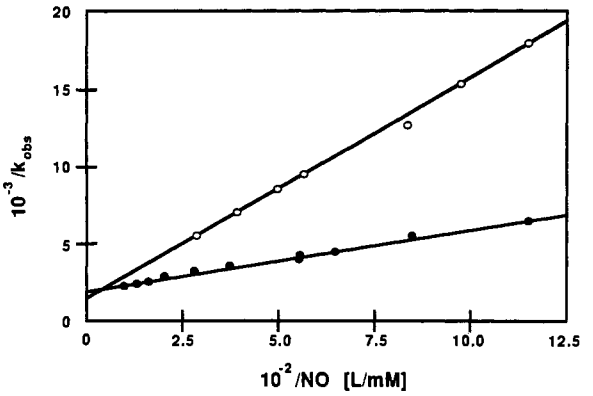

FIGURE 10: Double-reciprocal plot for NO pressure dependence of redox kinetics of (●) Hb_m(III)NO and (○) Mb(III)NO.

Competition between NO and His^{F8} imidazole for the proximal coordination site would occur at this juncture. The coordination of the iron atom by imidazole-F8 and removal of $(NO)_2^+$ (presumably to yield NO_2^-) are followed by rapid binding of NO to give the product heme(II) nitrosyl P.

The hypothesis that $(NO)_2^+$ may be released from D is supported by the formation of NOF via reaction of Hb_A(III)F with NO (Benko & Nai-Teng, 1983) and of CH_3ONO from CH_3OH and ClFe(OEP)NO (Wayland & Olson, 1974). Reduction of the ClFe(OEP)NO model indeed proceeds more quickly when imidazoles are used, these being stronger nucleophiles than CH_3OH. The decrease in rate observed at increased p_{NO} would now correspond to the formation of dinitrosyl E being inhibitory of this pathway. The total ferric heme is distributed between C and E, so that the rate equation becomes

$$-d[Hb(III)NO]/dt = k_3[Hb(III)NO][NO]/(1 + K_2[NO])$$

with k_1' now approaching $k_3[NO]$ in the lower and k_3/K_2 in the higher [NO] limits.

There are three observations that hold, regardless of mechanism.

(i) By analogy with its tensioning effect on the Fe–N_{His} bond of Hb_A(II)NO (Szabo & Perutz, 1976), the fact that DPG accelerates the rate of reduction in the case of Hb_A is taken as evidence that His^{F8} vacates the axial position in the rate-determining step, as is required by both pathways.

(ii) Direct evidence for the generation of E is provided by difference spectroscopy of Hb_m(III)NO under 4 atm of NO, which reveals the generation of a species with α/β-region absorptions at 527 and 562 nm. We assign this as the *trans*-dinitrosylheme, by direct comparison with Fe(PPIXDME)$(NO)_2^+$ (Table I). This complex [or Fe(OEP)$(NO)_2^+ClO_4^-$] and Fe(OEP)$NO^+ClO_4^-$ (formed under an NO/N_2 mixture) together model the event that gives the equilibrium constant K_2.

(iii) The data are linearized (Figure 10) by a reciprocal plot of the pseudo-first-order rate constants ($1/k_1'$) for Hb_m and Mb as a function of the reciprocal nitric oxide concentration (1/[NO]). The intercept reflects the decrease in rate at higher [NO], and the plot yields slope and intercept respectively of $1/(K_2k_4)$ and $1/k_4$ for the first mechanism or of $1/k_3$ and K_2/k_3 for the second mechanism. The corresponding values are in Table V.

The low values of K_2 are not unexpected. Although the Hb_m K_2 value for the first mechanism agrees with our estimate from the difference spectroscopy, the implied stability of the dinitrosyl is surprising, because Fe(OEP)$(NO)_2^+$ and Fe(PPIXDME)$(NO)_2^+$ are stable (toward dissociation) only in noncoordinating solvent under NO, while in the protein proximal imidazole competes with NO. As to the differences in rates among the various proteins studied here, we note that there appears to be a correlation between the relative rates and the amino acid content of the distal environment. There are two types of interactions in complex D: (a) There is a steric repulsion between the heme pocket amino acids and the two nitrosyl groups (Deatherage et al., 1979). (b) At pH 7 there is a repulsive interaction with cationic side chains (Table VI), so that the formation of D may be disfavored and the rate of reduction decreases (Hb_α > Hb_m > Mb, Table VII).

Table VI: Amino Acids in Distal Environment

	C7	CD1	G5	G8	E7	E11	E14	E15
Hb_α	*Tyr*	Phe	Phe	Leu	His	Val	Ala	Leu
Hb_m	Lys	Phe	Phe	Leu	*Leu*	Val	*Glx*	*Ile*
Mb	Lys	Phe	Phe	*Ile*	His	Val	Ala	Leu

Table VII: Temperature Dependence of Rates

	$10^4k_1'$ (s^{-1})			
temp (°C)	Hb_αNO	Hb_mNO	MbNO	Hb_ANO
5	2.11	0.69	0.28	0.12
10	3.23	1.08	0.45	0.13
15	4.33	1.84	0.66	0.14
20	5.96	2.17	1.04	0.17
25	9.03	3.75	1.52	0.18
σ	±0.03	±0.04	±0.05	±0.02

Table VIII: Activation Parameters

heme	$\Delta G^\ddagger$ (kJ·mol^{-1})	$\Delta H^\ddagger$ (kJ·mol^{-1})	$\Delta S^\ddagger$ (J·mol^{-1}·K^{-1})	$E_a^\ddagger$ (kJ·mol^{-1})
Hb_ANO "recycled"	83.7	26.9	−193	29.3
Hb_αNO	74.7	59.1	−53	61.5
MbNO	79.0	70.6	−29	73.0
Hb_mNO	76.8	70.1	−23	72.5
σ^a	±2.3	±0.8	±5	±2.4

[a] From analysis only of random errors.

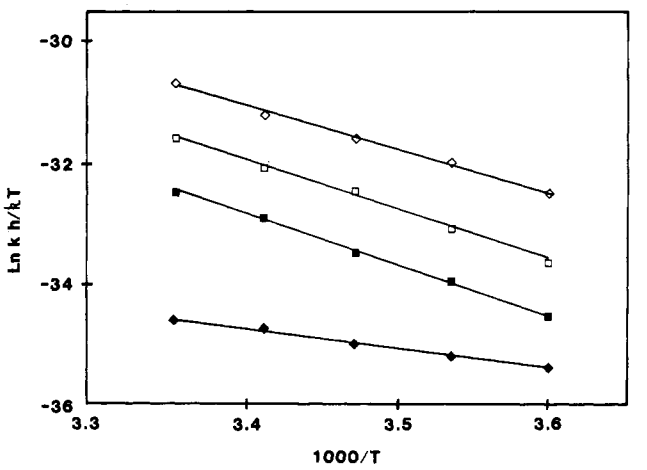

FIGURE 11: Eyring plots for (□) Hb_m, (■) Mb, (◇) Hb_α, and (◆) "recycled" Hb_A. The derived activation parameters entail the approximation $(1 + K_2[NO]) \approx 1$; the [NO] values are $\sim 10^{-3}$ M.

Activation Parameters. The temperature dependences of the rates (Table VII) are shown as Eyring plots of $k_1'/[NO]$ (Figure 11). The derived parameters, $\Delta G^\ddagger$, $\Delta H^\ddagger$, and $\Delta S^\ddagger$, which should be associated with k_3, are given in Table VIII. The $\Delta H^\ddagger$ values would include the contribution from the energy required for rupturing the Fe–N_{His} bond, as well as a crystal field activation energy term (C → D).

The negative entropies of activation also seem nicely consistent with the associative mechanism proposed. In the case of Hb_mNO, the absence of distal histidine may lead to a greater degree of rotational mobility for bound NO, resulting in a $\Delta S^{\ddagger}$ less negative than for the other proteins, while the relatively large value of $\Delta S^{\ddagger}$ (and of $\Delta H^{\ddagger}$) for tetrameric Hb_ANO suggests that more than one NO molecule (and thus more than one subunit) is involved in the rate-determining step ($\Delta S^{\ddagger}$ of $Hb_ANO \approx 4\Delta S^{\ddagger}$ of $Hb_\alpha NO$).

ACKNOWLEDGMENTS

We are indebted to Dr. E. M. Brown (USDA-ERRC) for assistance with obtaining and processing the CD data. We thank Drs. A. L. Crumbliss, M. P. Doyle, and B. B. Wayland for helpful discussion and Drexel University for support.

REFERENCES

Addison, A. W., & Dougherty, P. L. (1982) *Comp. Biochem. Physiol., B: Comp. Biochem. 72B*, 433–438.

Addison, A. W., & Burman, S. (1985) *Biochim. Biophys. Acta 828*, 362–268.

Addison, A. W., Canella, K. A., & Dougherty, P. L. (1980) *Abstracts of Papers*, 180th National Meeting of the American Chemical Society, Las Vegas, NV, BIOL 203, American Chemical Society, Washington, D.C.

Ainscough, E. W., Addison, A. W., Dolphin, D., & James, B. R. (1978) *J. Am. Chem. Soc. 100*, 7585–7591.

Antipas, A., Buchler, J. W., Gouterman, M., & Smith, P. D. (1978) *J. Am. Chem. Soc. 100*, 3015–3024.

Armor, J. N. (1974) *J. Chem. Eng. Data 19*, 82–84.

Ascenzi, P., Giacometti, G. M., Antonini, E., Rotilio, G., & Brunori, M. (1981) *J. Biol. Chem. 256*, 5383–5386.

Benko, B., & Yu, N.-T. (1983) *Proc. Natl. Acad. Sci. U.S.A. 80*, 7043–7046.

Bucci, E., & Fronticelli, C. (1965) *J. Biol. Chem. 240*, 551–552.

Chien, J. C. W. (1969) *J. Am. Chem. Soc. 91*, 2166–2168.

Cotton, F. A., & Wilkinson, G. (1980) in *Advanced Inorganic Chemistry*, pp 90, Wiley-Interscience, New York.

Deatherage, J. F., & Moffat, K. (1979) *J. Mol. Biol. 134*, 401–417.

Dickinson, L. C., & Chien, J. C. W. (1971) *J. Am. Chem. Soc. 93*, 5036–5040.

Doetschman, D. C., Schwartz, S. A., & Utterback, S. G. (1980) *Chem. Phys. 49*, 1–8.

Eaton, W. A., Hanson, L. K., Stephens, P. J., Sutherland, J. C., & Dunn, J. B. R. (1978) *J. Am. Chem. Soc. 100*, 4991–5001.

Ehrenberg, A., & Szczepkowski, T. W. (1960) *Acta Chem. Scand. 14*, 1684–1692.

Fish, R. H., Homstead, R. L., & Gaffield, W. (1976) *Tetrahedron 32*, 2689–2692.

Gillard, R. D. (1968) in *Physical Methods in Advanced Inorganic Chemistry* (Hill, H. A. O., & Day, P., Eds.) pp 167–213, Wiley-Interscience, London.

Goedken, V. L., Dessy, G., Ercolani, C., Fares, V., & Gastaldi, L. (1985) *Inorg. Chem. 24*, 991–995.

Guilard, R., Fontess, M., & Fournari, P. (1976) *J. Chem. Soc., Chem. Commun.*, 161–162.

Hildebrand, J. H., Prausnitz, J. M., & Scott, R. L. (1970) *Regular and Related Solutions*, Chapter 8, Van Nostrand-Reinhold, New York.

Hoffman, B. M., & Gibson, Q. H. (1978) *Proc. Natl. Acad. Sci. U.S.A. 75*, 21–25.

Hoffman, B. M., Weschler, C. J., & Basolo, F. (1976) *J. Am. Chem. Soc. 98*, 5473–5482.

Hawn, G. G., Maricondi, C., & Douglas, B. E. (1979) *Inorg. Chem. 18*, 2542–2547.

Hsu, M. C., & Woody, R. W. (1971) *J. Am. Chem. Soc. 93*, 3515–3524.

Imamura, T., Baldwin, T. O., & Riggs, A. (1972) *J. Biol. Chem. 247*, 2785–2797.

Kandler, R. L., Constantinidis, I., & Satterlee, J. D. (1984) *Biochem. J. 226*, 131–138.

Keilin, D., & Hartree, E. F. (1937) *Nature (London) 139*, 548–563.

Linn, S. H., Ono, Y., & Ng, C. Y. (1981) *J. Chem. Phys. 74*, 3342–3347.

London, H., & Bonnet, M. J. (1979) *J. Chem. Soc., Chem. Commun.*, 702–704.

Mackin, T. H. C., Benko, B., Yu, N. T., & Gersonde, K. (1983) *FEBS Lett. 158*(2), 199–202.

McCandlish, E., Miksztal, A. R., Nappa, M., Sprenger, A. W., Stong, J. D., & Spiro, T. G. (1980) *J. Am. Chem. Soc. 102*, 4268–4271.

Melia, T. P. (1965) *J. Inorg. Nucl. Chem. 27*, 95–98.

Mentzen, B. F., Bonnet, M. C., & London, H. (1980) *Inorg. Chem. 19*, 2061–2066.

Mertis, K., & Wilkinson, C. (1976) *J. Chem. Soc., Dalton Trans.*, 1488–1492.

Müller, E. H., & Rundel, W. (1960) *Chem. Ber. 93*, 1541–1549.

O'Connor, E. R. P., Harrington, J. P., & Herskovits, T. T. (1980) *Biochim. Biophys. Acta 624*, 346–362.

O'Keeffe, D. H., Ebel, R. E., & Peterson, J. A. (1978) *J. Biol. Chem. 253*, 3509–3516.

Otsuka, J. (1966) *J. Phys. Soc. Jpn. 21*, 596–620.

Padlan, E. A., & Love, W. E. (1974) *J. Biol. Chem. 249*, 4067–4078.

Platt, J. R. (1956) in *Radiation Biology* (Hollaender, A., Ed.) Vol 3, pp 71–123, MacGraw-Hill, New York.

Porterfield, W. W. (1984) in *Inorganic Chemistry*, p 447, Addison-Wesley, Reading, MA.

Rifkind, J. M., Lauer, L. D., Chiang, S. C., & Li, N. C. (1976) *Biochemistry 15*, 5337–5343.

Sancier, K. M., Freeman, G., & Mills, J. S. (1962) *Science (Washington, D.C.) 137*, 752–754.

Satterlee, J. D. (1984) *Biochim. Biophys. Acta 791*, 384–394.

Scheidt, W. R., & Piciulo, P. L. (1976) *J. Am. Chem. Soc. 98*, 1913–1926.

Scheidt, W. R., Lee, Y. J., & Hatano, K. (1984) *J. Am. Chem. Soc. 106*, 3191–3198.

Seamonds, B., Forster, R. E., & George, P. (1971) *J. Biol. Chem. 246*, 5391–5397.

Sharma, V. S., Isaacson, R. A., John, M. E., Waterman, M. R., & Chevion, M. (1983) *Biochemistry 22*, 3897–3902.

Shaw, A. W., & Vosper, A. J. (1977) *J. Chem. Soc., Faraday Trans. 1*, 1239–1244.

Smith, D. W., & Williams, R. J. P. (1970) *Struct. Bonding (Berlin) 7*, 1–45.

Szabo, A., & Perutz, M. F. (1976) *Biochemistry 15*, 4427–4428.

Tamura, M., Kobayashi, K., & Hayashi, K. (1978) *FEBS Lett. 88*, 124–126.

Trittelvitz, E., Gersonde, K., & Winterhalter, K. H. (1975) *Eur. J. Biochem. 51*, 33–42.

Waks, M., Yip, Y. K., & Beychock, S. (1973) *J. Biol. Chem. 248*, 6462–6470.

Wayland, B. B., & Olson, L. W. (1974) *J. Am. Chem. Soc. 96*, 6037–6042.
Wayland, B. B., Minkiewicz, J. V., & Abd-El Maged, M. E. (1974) *J. Am. Chem. Soc. 96*, 2795–2801.
Welborn, C. H., Dolphin, D., & James, B. R. (1981) *J. Am. Chem. Soc. 103*, 2869–2871.
Yonetani, T., Yamamoto, H., Erman, J. E., Leigh, J. S., Jr., & Reed, G. H. (1972) *J. Biol. Chem. 247*, 2447–2455.
Yoshimura, T., Ozaki, T., Shintani, Y., & Watanabe, H. (1971) *Arch. Biochem. Biophys. 193*, 301–313.
Zerner, M., Gouterman, M., & Kobayashi, H. (1966) *Theor. Chim. Acta. 6*, 363–400.

Use of Substituted (Benzylidineamino)guanidines in the Study of Guanidino Group Specific ADP-ribosyltransferase†

Gopalan Soman, Jayashree Narayanan, Bruce L. Martin, and Donald J. Graves*
Department of Biochemistry and Biophysics, Iowa State University, Ames, Iowa 50011
Received January 9, 1986; Revised Manuscript Received March 12, 1986

ABSTRACT: A number of substituted (benzylidineamino)guanidines with different substitutents in the benzene nucleus are synthesized by coupling substituted benzaldehydes with aminoguanidine, and these compounds are tested as substrates for cholera toxin catalyzed ADP-ribosylation. A spectrophotometric assay method for the measurement of ADP-ribosyltransferase activity is developed, making use of the absorption characteristics of some of these compounds and the difference in the ionic character of the free compounds and the ADP-ribosylated products. The kinetic parameters for the ADP-ribosylation of these compounds are evaluated. A correlation between log k_{cat} or log (k_{cat}/K_m) and the Hammett substituent constant σ is observed. This correlation suggests the importance of substrate electronic effects on the enzymatic reaction. The reactivity of these compounds as acceptors of ADP-ribosyl groups in the reaction catalyzed by cholera toxin increases with increasing electron-donating power of the substituents in the benzene function. The effect is primarily on the catalytic rate constant, k_{cat}, not on the binding constant, K_m. The results are consistent with an S_N2 reaction mechanism in which the deprotonated guanidino group makes a nucleophilic attack on the C-1 carbon of the ribose moiety.

Cholera toxin (Moss & Vaughan, 1977; Moss & Richardson, 1978; Moss et al., 1976), *Escherichia coli* enterotoxin (Moss & Richardson, 1978; Moss et al., 1979), and ADP-ribosyltransferases from different animal sources (Moss & Vaughan, 1978; Beckner & Blecher, 1981; Moss & Stanley, 1981a,b; Richter et al., 1983; Tanigawa et al., 1984; Soman et al., 1984a) are capable of transferring an ADP-ribosyl moiety from NAD[1] to functional groups in cellular proteins and also to simple guanidino compounds. The site of self-ADP-ribosylation in cholera toxin and the cholera toxin catalyzed ADP-ribosylation in transducin has been established to be arginyl residues (Xia et al., 1984; Van Dop et al., 1984). Though the functional residues modified in other proteins by cholera toxin and other ADP-ribosyltransferases are not well established, enzymes that use guanidino compounds as substrates are presumed to be guanidino group specific. Because of the recent reports indicating the presence of the ADP-ribosyltransferase activity in different animal and plant tissues (Moss & Vaughan, 1978; Beckner & Blecher, 1981; Moss & Stanley, 1981a,b; Richter et al., 1983; Tanigawa et al., 1984; Soman et al., 1984a; Pope et al., 1985), there is growing interest in these reactions as a means of posttranslational covalent modification of cellular proteins. But very little information is available on the natural protein substrates for these enzymes, on the precise physiological role of these reactions, and also on the enzymology of the process. In the absence of well-defined natural substrates, much information may be derived from studies using model substrates. Earlier studies on cholera toxin reveal that introduction of negatively charged groups near the guanidino group is unfavorable for binding (Moss & Vaughan, 1977). Thus, arginine itself is a very poor substrate for ADP-ribosylation by cholera toxin, but blocking the carboxyl group as in L-arginine methyl ester or replacing the carboxyl group by a methyl group as in agamatine makes the derivatives much better substrates for cholera toxin and other ADP-ribosyltransferases (Moss & Vaughan, 1977; Moss et al., 1983). A recent report suggests that, in a series of guanidino compounds tested, the ADP-ribosyltransferase activity, as measured by the ability of the compounds to release nicotinamide, increases with increasing hydrophobicity of the compounds (Tait & Nassau, 1984). Thus, both electronic effects and hydrophobicity seem to influence the reactivity of the ADP-ribosyltransferases.

Recently, we have reported that the guanylhydrazones, [(*p*-nitrobenzylidine)amino]guanidine and methylglyoxal

† This work was supported by Research Grant GM34262-01 from the National Institutes of Health, U.S. Public Health Service. This is Journal Paper J-12138 of the Iowa Agriculture and Home Economics Experiment Station, Ames, IA, Project 2120.
* Author to whom correspondence should be addressed.

[1] Abbreviations: TEAA, triethylammonium acetate; BAG, (benzylidineamino)guanidine; DEA, diethylamino; DMA, dimethylamino; NBAG, [(*p*-nitrobenzylidine)amino]guanidine; HPLC, high-performance liquid chromatography; TCA, trichloroacetic acid; LAME, L-arginine methyl ester; NAD, nicotinamide adenine dinucleotide; DTE, dithioerythritol; Tris-HCl, tris(hydroxymethyl)aminomethane hydrochloride.

0006-2960/86/0425-4113$01.50/0